LBL-11822
Preprint

Lawrence Berkeley Laboratory
UNIVERSITY OF CALIFORNIA

Materials & Molecular
Research Division

Submitted to the Journal of Chemical Physics

PHOTOELECTRON ANGULAR DISTRIBUTIONS OF H_2O

C.M. Truesdale, S. Southworth, P.H. Kobrin,
D.W. Lindle, G. Thornton, and D.A. Shirley

August 1981

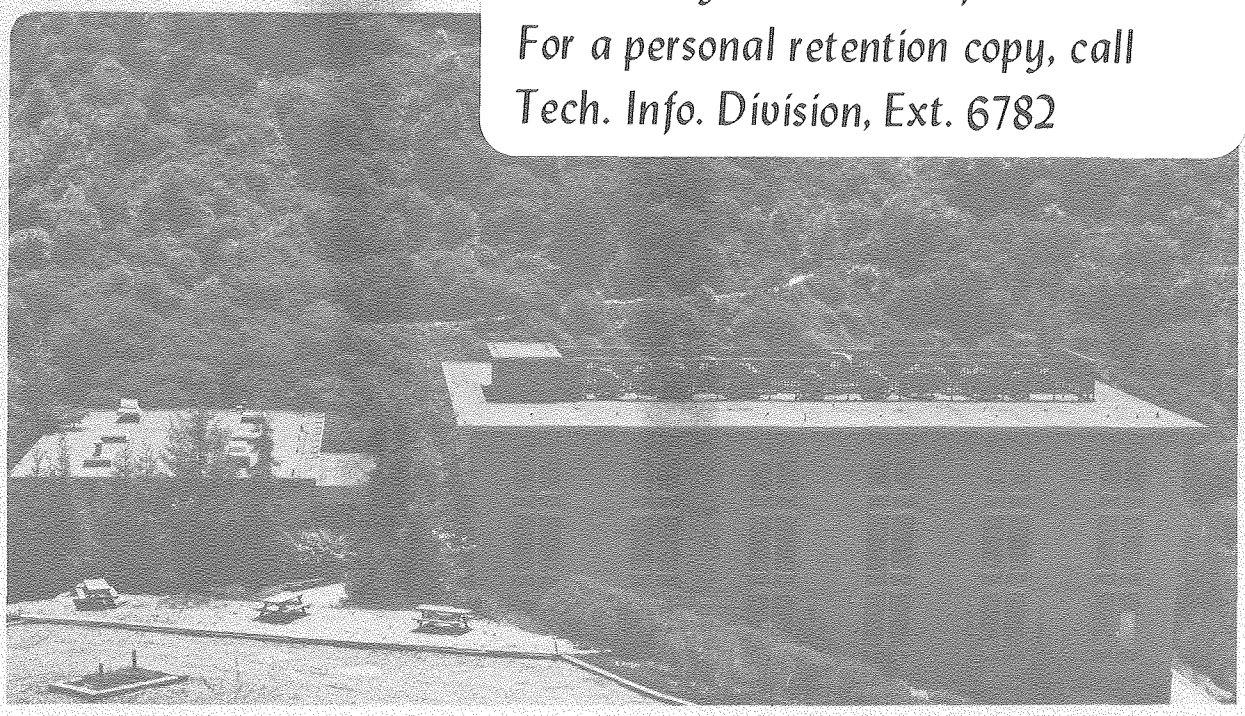

Prepared for the U.S. Department of Energy under Contract W-7405-ENG-48

DISCLAIMER

LBL-11822

PHOTOELECTRON ANGULAR DISTRIBUTIONS OF H_2O

C. M. Truesdale, S. Southworth, P. H. Kobrin, D. W. Lindle,
G. Thornton, and D. A. Shirley

Materials and Molecular Research Division
Lawrence Berkeley Laboratory
Department of Chemistry
University of California
Berkeley, California 94720

This work was supported by the Director, Office of Energy Research, Office of Basic Energy Sciences, Chemical Sciences, Division of the U.S. Department of Energy under Contract No. W-7405-ENG-48.

PHOTOELECTRON ANGULAR DISTRIBUTIONS OF H_2O

C. M. Truesdale, S. Southworth, P. H. Kobrin, D. W. Lindle,
G. Thornton,* and D. A. Shirley

Materials and Molecular Research Division
Lawrence Berkeley Laboratory
Department of Chemistry
University of California
Berkeley, California 94720

ABSTRACT

The partial cross-section and asymmetry parameters of the $^2B_1$, $^2A_1$ and $^2B_2$ ionic states of H_2O^+ have been measured at photon energies of 18-31 eV, by time-of-flight photoelectron spectroscopy using synchrotron radiation. The atomic character of the molecular orbitals is discussed in the interpretation of similarities and differences between the measurements for these states. Other synchrotron radiation data, resonance line measurements, and (e,2e) dipole results are included. A multiple-scattering Xα (MSXα) calculation and a ground-state inversion method calculation are in good agreement with our cross-section measurements. There is excellent agreement between experimental asymmetry parameters and those computed from the MSXα method. Stieltjes-Tchebycheff imaging model calculations suggest the presence of resonant channels. This may be the origin of weak resonance structure present in the measurements.

---

*Permanent address: Department of Chemistry, University of Manchester, Manchester M13-9PL, England

I. INTRODUCTION

Photoionization of the water molecule is a reaction of very wide interest. As in any photoionization process to which Yang's criteria[1] of initial-state random orientation and dipole multipolarity apply, and where the spin of photoelectrons is not detected, two parameters must be measured to describe photoionization to a given ionic state through a given channel.[2] These are the angle-integrated cross-section, $\sigma(\varepsilon)$, and the asymmetry parameter $\beta(\varepsilon)$, where ε is the photoelectron kinetic energy. If θ denotes the angle between the photoelectron propagation direction and the polarization vector of the exciting radiation, the differential cross-section for excitation by plane-polarized photons takes the form

$$\frac{d\sigma(\varepsilon)}{d\Omega} = \frac{\sigma(\varepsilon)}{4\pi} [1 + \beta(\varepsilon)P_2(\cos\theta)] , \qquad (1)$$

where $P_2(\cos\theta)$ is the second Legendre polynomial, equal to $\frac{1}{2}(3\cos^2\theta - 1)$. Thus, the photoionization of H_2O can be characterized by measuring $[d\sigma(\varepsilon)/d\Omega]$ at two or more ejection angles for the various photoionization channels, each of which corresponds to ejection of an electron from a particular molecular orbital. $\beta(\varepsilon)$ characterizes the angular distribution of the photoelectrons. The complementary measurement of photoelectron spin polarization, in addition to $\sigma(\varepsilon)$ and $\beta(\varepsilon)$, would completely describe the photoionization process.[3]

In this paper we report $\sigma(\varepsilon)$ and $\beta(\varepsilon)$ measurements for the processes

$$H_2O + h\nu \rightarrow H_2O^+ (^2B_1, 1b_1^{-1}) + e^- \quad (2a)$$

$$H_2O + h\nu \rightarrow H_2O^+ (^2A_1, 3a_1^{-1}) + e^- \quad (2b)$$

and

$$H_2O + h\nu \rightarrow H_2O^+ (^2B_2, 1b_2^{-1}) + e^- \quad (2c)$$

for photon energies in the range $h\nu$ = 18–31 eV. These measurements are compared with previous experimental results and with theory.

The experimental procedures are described in Section II. Results are presented and discussed in Section III and conclusions are given in Section IV.

II. EXPERIMENTAL

The experiments were performed at the Stanford Synchroton Radiation Laboratory, on the VUV beam line.[4] This source provides highly (>97 percent)[4] linearly polarized radiation. The time structure of this source (0.3 nsec pulse length, with a 780 nsec period) facilitated the use of a specially designed time-of-flight (TOF) detector.[5] These experiments were performed with a 2.7Å (FWHM) monochromator band pass throughout the available radiation energy range of 18–31 eV.

The TOF detectors provide major advantages for measurements of $\sigma(\varepsilon)$ and $\beta(\varepsilon)$ at low resolution. The entire spectrum is collected

simultaneously at each photon energy, thereby enhancing the sensitivity, and the low duty cycle at each photoelectron kinetic energy enhances the signal/noise ratio. Two detectors are used, at angles $\theta = 0^\circ$ and $\theta = 54.7^\circ$ relative to the polarization direction. At the "magic angle" of 54.7°, P_2 vanishes and the $d\sigma(\varepsilon)/d\Omega$ measurement yields $\sigma(\varepsilon)$. Measurement of the relative intensities of electrons collected in the 0° and 54.7° spectra yields $\beta(\varepsilon)$. We note that simultaneous data collection at two angles is intrinsically a more reliable method for obtaining $\beta(\varepsilon)$ than measurements based on moving a single detector to several angles. Not only are errors in reproducing the detector placements avoided, but fluctuations in photon beam intensity and sample gas density during each counting period are totally compensated. The remaining principal sources of systematic error--relative detector efficiency for $\beta(\varepsilon)$ measurements and transmission of the 54.7° detector for $\sigma(\varepsilon)$ measurements--are dealt with in a calibration procedure.

As calibration gases we used helium and a rare gas mixture of argon, krypton, and xenon. The asymmetry parameters for these gases were taken from previous resonance-line and synchrotron-radiation measurements.[6,7] Both the relative efficiencies of the two detectors and the transmission of the 54.7° detector over the relevant electron kinetic-energy range were thereby obtained. The calibration gases and sample gas (H_2O) were introduced into the sample chamber, through an inlet probe described previously.[5] The sample density in the interaction region was taken as being proportional to the backing pressure, which was monitored by a capacitance manometer.[5] The photon intensity

was monitored by a sodium salicylate scintillator, phototube, and picoammeter. For each counting period (typically 1000 sec), the relative photon flux and sample pressure were integrated and stored on scalers. The backing pressure for the gases was nominally 3 torr. A typical TOF spectrum for the outer three molecular orbitals of H_2O is shown in Fig. 1.. There is good separation of the molecular orbital peaks, but vibrational structure is not resolved.

Data reduction is straightforward because of the calibration procedure. A more detailed description of this procedure has been given by Southworth, et al.[8] Briefly, $\beta(\varepsilon)$ values are determined from the ratio of the peak areas measured at 0° ($A(0°,\varepsilon)$) and 54.7 ($A(54°,\varepsilon)$) and the relative collection efficiency ($f_0(\varepsilon)$) of the two detectors.

$$\beta_0(\varepsilon) = -1 + \frac{A(0°,\varepsilon)/A(54°,\varepsilon)}{f_0(\varepsilon)} \qquad (3)$$

The $\beta_0(\varepsilon)$ measurements are corrected for the 3 percent unpolarized photon beam component, for angle-averaging over the finite source region and the collection solid angles, and for the difference between the measured $\beta(\varepsilon)$ value and that of the calibration photoelectron line. It should be noted that because of the internal calibration procedure performed, the derived asymmetry parameters are only rather weakly dependent on the degree of polarization of the radiation, on geometrical parameters of the interaction and detection system, and on certain experimental systematic errors.[8]

Peak areas measured at 54.7°, after normalization for sample density, photon intensity, and transmission of the 54.7° detector, were corrected in an analogous fashion to the $\beta(\varepsilon)$ values to yield relative partial cross-sections. These were then scaled to yield absolute partial cross-sections by the use of the total photoabsorption cross-sections measured by L. de Reilhac and N. Damany[9] and the ionization efficiencies reported by Katayama, et al.[10]

III. RESULTS AND DISCUSSION

At this early stage in the development of theories of molecular photoionization, any discussion of molecular $\sigma(\varepsilon)$ and $\beta(\varepsilon)$ parameters must be somewhat tentative. Therefore, comparisions of results from different experimental and theoretical sources must perforce be an implicit evaluation of the methods employed by those sources. Thus, in the context of discussing our results we are addressing methodologies as well as the physical properties of the water molecule.

The ground-state electronic configuration of water is $(1a_1)^2\ (2a_1)^2\ (1b_2)^2\ (3a_1)^2\ (1b_1)^2$. In the UV range available, the $1a_1$ and $2a_1$ electrons are too strongly bound to be ejected. The other three orbitals can be ionized according to the channels in Eq. 2. In Table I, we present the partial cross-sections and asymmetry parameters for these three channels in the photon energy range 18–31 eV. Also shown for comparison are $\beta(\varepsilon)$ values at $h\nu$ = 21.2 eV, reported by Carlson and McGuire[11] and by Katsumata, Achiba, and Kimura,[12] and the $\sigma(\varepsilon)$ measurements at 21.2, 23.5, and 24.5 eV

reported by Katsumata, et al. and dipole (e,2e) results of Tan, Brion, van der Leeuw, and van der Wiel.[13] The agreement is good.

Before separately discussing our results for the three channels, we note a strong similarity among them. This arises, as Roche, Salahub, and Messmer[14] have pointed out, because the $1b_1$, $3a_1$, and $1b_2$ molecular orbitals are all derived from the O 2p shell. Banna and Shirley carried this analogy further in discussing photoemission from the second-row hydrides,[15] noting both their conceptual derivation from neon and the dominant contribution of the second-row atom's valence orbitals (rather than a hydrogen "1s" orbital) to the photoemission cross-sections. Roche, et al.[14] computed $\sigma(\varepsilon)$ and $\beta(\varepsilon)$ values for O 2p to compare with their H_2O molecular-orbital $\sigma(\varepsilon)$ and $\beta(\varepsilon)$ results, which are based on the multiple-scattering $X\alpha$ method.[16,17] Thus, the strong similarity among the $\sigma(\varepsilon)$ and $\beta(\varepsilon)$ curves (Figs. 2, 3, and 4) for the three channels is the first qualitative success of this theoretical picture. A more quantitative measure of the success of $X\alpha$ computations is obtained by comparison with other theoretical curves and with experiment, as discussed below.

The lone-pair $1b_1$ orbital is least distorted from an atomic O 2p orbital by the presence of the atomic hydrogens because this orbital is orthogonal to the plane of the molecule and is nonbonding. As predicted,[14] both $\sigma(\varepsilon)$ and $\beta(\varepsilon)$ follow the atomic orbital curves quite closely as shown in Fig. 2. The observed ~60 percent increase of $\beta(\varepsilon)$ with increasing energy agrees well with the $X\alpha$ calculation, and the agreement of the $\beta(\varepsilon)$ behavior near the end points leaves

little to be desired. The MSXα calculation predicts a decrease of $\sigma(\varepsilon)$ by about 20 percent with increasing energy, although the absolute value of $\sigma(\varepsilon)$ is typically 20 percent higher than predicted. There is better agreement between our $\sigma(\varepsilon)$ results and Xα calculation below 20 eV photon energy.

The magnitude of $\sigma(\varepsilon)$ was predicted more accurately by Williams and Langhoff,[18] and by Hilton, Nordholm, and Hush.[19] The former calculation was based on the Stieltjes-Tchebycheff (ST) moment imaging theory,[20,21] and the latter is developed by use of the ground state inversion potential method (GIPM). The ST approach uses variational calculations of square-integrable wavefunctions of the photoelectron interacting with a non-local and noncentral molecular-ionic potential. It yields pseudospectra and oscillator strengths from which the cross-sections are derived by moment-imaging methods, but $\beta(\varepsilon)$ is not calculated because the continuum wavefunctions are not determined. It should, however, be capable of predicting structure in $\sigma(\varepsilon)$, a subject to be discussed latter. The ST calculation of Delaney, Saunders, and Hillier[22] is in only qualitative agreement with our results for predicting the decrease in $\sigma(\varepsilon)$ as a function of photon energy.

The GIPM calculation determines the molecular orbital cross-sections from those of the atomic subshell components. It can include the interference effects between the atomic components of the molecular orbital.[21] As stated, the calculations of Hilton, et al. predict $\sigma(\varepsilon)$ with rather good accuracy. Their model determined

that interference effects between the atomic components of the $1b_1$ molecular orbital are negligible.

We conclude our comments on the gross form and magnitude of $\sigma(\varepsilon)$ for the $^2B_1(1b_1^{-1})$ transition by noting that, although the (e,2e) data do not show any resonance structure, there is otherwise good qualitative agreement between our results and the (e,2e) data of Tan, et al.[13] throughout the range of our measurements. Maxima in our $\sigma(\varepsilon)$ data appear near 22 eV and 25 eV, and some structure is present below 20 eV. Dutuit, et al. reported photoelectron intensities for this state up to 20 eV, with structure at 19 eV, but their reported cross-sections are higher than ours in the small region of overlap.[23] Those authors suggest that the broad maximum at 19 eV may be due to a competition between neutral dissociation and autoionization to ionic states of H_2O. Wu and Judge, who reported recent measurements of Lyman α fluorescence of neutral dissociation products of H_2O, have suggested that a sharp structure present in absorption spectra at ~18.5 eV corresponds to an s-like Rydberg state, converging to the $^2B_2$ ionic channel, from which predissociation occurs.[24] This explanation accounts for resonance structure in, and competition between, the photoionization and dissociation channels.

The two ST calculations are somewhat different in detail, one being based on the time-dependent Hartree-Fock (TDHF) approximation[18] and the other on a static-exchange approximation,[22] and their resulting $\sigma(\varepsilon)$ curves differ as well. In particular, excitations of virtual

discrete states and states in the ionization continuum (e.g., $1b_1 \rightarrow 4a_1$) in the TDHF[18] calculation were found to yield maxima in the sub-channel cross-sections for the $^2B_1$ ($1b_1^{-1}$) channel. These maxima were smaller or absent in their final curves. A broad shape resonance centered around 22 eV photon energy due to excitation of a σ^*a_1 valence-like orbital predicted by Williams and Langhoff may identify the resonance structure located at ~22 eV in the present work. Figure 2 shows that Delaney et al.[22] also find structure in the $\sigma(\varepsilon)$ curve at ~18 eV for the $^2B_1$ state, but with small amplitude. The experimental resonance feature in $\sigma(\varepsilon)$ for the $^2B_1$ state below 20 eV may also result from the shape resonance predicted by Delaney, et al. Until confirmatory measurements are made it seems prudent to defer further interpretation.

The $\beta(\varepsilon)$ parameter for the $^2B_1$ ($1b_1^{-1}$) channel has been measured previously only at fixed energies (see Table I), and has been calculated only by Roche, et al. As noted above, agreement between experiment and theory is excellent, except for the structure near $h\nu$ = 22 eV and 25 eV, as in $\sigma(\varepsilon)$. In particular, $\beta(\varepsilon)$ starts relatively high (0.76) at $h\nu$ = 18 eV, rises quickly to 1.0 by $h\nu$ = 20 eV, and (except for the structure near 22 eV and 25 eV) remains large and increases to ~1.4 near 30 eV, in good accord with the Xα results.

Results for the $^2A_1(3a_1^{-1})$ channel are shown in Fig. 3. There is good agreement among our measurements, the results of Dutuit, et al.[23]

above 22 eV, and the (e,2e) results[13] for the entire photon energy range. This channel involves the "O 2p-like" orbital, which is in-plane and directed along the C_{2v} axis. It has significant involvement with the hydrogen atoms. This fact is evident in photoemission. For example, in earlier work[15] the $^2A_1$ intensity was shown to increase much more between spectra excited by soft-x-ray radiation (132.3 eV) and those excited by higher energies (1487 eV) than did those of the $^2B_1$ or $^2B_2$ states. This suggests that O 2s admixture is present in the $3a_1$ orbital. We interpret this as being due to sp hybridization, which is allowed by symmetry. Thus, unlike the $1b_1$ and $1b_2$ orbitals, the $3a_1$ orbital does not have a nodal plane through the oxygen nucleus.

There is little difference between the present experimental $\sigma(\varepsilon)$ values for the $^2B_1$ $(1b_1^{-1})$ and $^2A_1$ $(3a_1^{-1})$ states, although the calculated $\sigma(\varepsilon)$ values of Roche, et al. are somewhat higher for the $^2A_1$. On the average, the Xα calculation is somewhat closer to experiment than the ST[18,22] or GIPM[19] results. The GIPM calculation that includes interference effects for the $^2A_1$ channel is presented in Fig. 3: the GIPM calculation without interference effects would be in better agreement with the present results, judging from the four points given by Hilton, et al.[19] The GIPM $\sigma(\varepsilon)$ curve shown in Fig. 3 predicts a broad maximum near 20 eV.[19] Delaney, et al.[22] predict a resonance at ~19 eV. Williams and Langhoff[18] predicted that a continuum subchannel resonance ~25 eV is present for the excitation

into the continuum $\sigma^* a_1$ orbital. The experimental structure falls at ~18 eV, ~22 eV, and ~25 eV.

The prediction of $\beta(\varepsilon)$ for the $^2A_1$ $(3a_1^{-1})$ ionic state is a success for the Xα model. The theoretical curve starts at a low value of 0.6 at $h\nu$ = 18 eV and rises to a value of 1.2 near $h\nu$ = 31 eV, in good overall agreement with the data. This behavior is to be contrasted to the $\beta(\varepsilon)$ curve for the $^2B_1$ $(1b_1^{-1})$ channel discussed above. The two $\beta(\varepsilon)$ curves are quite different in detail, as a careful comparison will show, and on a coarse scale the predicted differences are closely followed experimentally. The difference of the $^2A_1$ $(3a_1^{-1})$ $\beta(\varepsilon)$ curve from that for the $^2B_1$ $(1b_1^{-1})$ state, which closely follows the differences from the $\beta(\varepsilon)$ curve of an O 2p orbital, can be attributed to perturbations of the O 2p orbital by the hydrogens, leading to hybridization. Table II presents the theoretical $\beta(\varepsilon)$ and experimental difference between $^2B_1$ and $^2A_1$ ionic states of H_2O. Both the experimental and the theoretical average differences $\Delta\beta$ for these two states are ~0.3 β unit. The Xα calculation is in excellent agreement with experiment in predicting this molecular bonding effect. Again weak resonance-like structure is found in $\beta(\varepsilon)$ at $h\nu$ = 20 eV and 24 eV.

The $^2B_2$ $(1b_2^{-1})$ cross-section is larger than those of the other two states as shown in Fig. 4, which is consistent with a larger difference of this O-H bonding orbital from an O 2p orbital. The Xα calculation predicts this result well,[14] while the GIPM curve is low and the ST calculations[18,22] are typically 30-50 percent higher than

experiment. Our data agree well with the (e,2e) results[13] and with Dutuit, et al.[23] There appears to be two small resonances in our data at ~22 eV and ~25 eV. Williams and Langhoff[18] predict a broad subchannel resonance centered around 25 eV due to transitions into a $\sigma^* a_1$ orbital in the continuum, but no maximum appears in the final $\sigma(\epsilon)$ curve. Cross-section measurements of Dutuit, et al. seem to confirm that there is structure near 22 eV.[23] The ST calculations of Delaney, et al.[19] also predict a resonance feature near ~23 eV.

The $\beta(\epsilon)$ parameter for the $^2B_2$ ($1b_2^{-1}$) channel is much lower than for the other two channels and for the O 2p orbital, owing to its strong molecular O-H bonding character. The $\beta(\epsilon)$ value increases smoothly from -0.1 to 0.6 as $h\nu$ increases from 21 eV to 30 eV. This behavior is well predicted by the Xα model, which is in very good agreement at the high-energy end.

IV. CONCLUSIONS

Several conclusions can be drawn from this work:

1. The $\sigma(\epsilon)$ and $\beta(\epsilon)$ parameters for the $^2B_1$ ($1b_1^{-1}$), $^2A_1$ ($3a_1^{-1}$), and $^2B_2$ ($1b_2^{-1}$) channels in the photoionization of H_2O correspond with the parameters for O 2p orbitals from which these molecular orbital are derived. The $\sigma(\epsilon)$ and $\beta(\epsilon)$ parameters are sensitive to chemical bonding.
2. The Xα calculation of Roche, et al. predicts the overall form of $\sigma(\epsilon)$ and $\beta(\epsilon)$ for these orbitals very well.

3. The GIPM calculation of Hilton, et al. predicts $\sigma(\varepsilon)$ equally well, on the average.
4. The two available ST calculations predict $\sigma(\varepsilon)$ values which tend to be somewhat higher than experiment.
5. Our work agrees well overall with the (e,2e)-derived $\sigma(\varepsilon)$ results of Tan, et al.; however, their results do not show any structure.
6. Our measurements show weak resonance-like structure in both $\sigma(\varepsilon)$ and $\beta(\varepsilon)$, as do the results of Dutuit, et al. There is good qualitative agreement with Dutuit, et al. at photon energies higher than 21 eV.
7. The ST models show resonances in the ionization sub-channels, corresponding to excitation of virtual discrete orbitals imbedded in the continuum. The location of broad continuum resonances predicted by Williams and Langhoff may identify the underlying resonance structure present in our data at 22 eV for the $^2B_1$, and 25 eV vor the $^2A_1$ and $^2B_2$ ionic states calculations of Delaney, et al. give further indication that the ST method may possibly determine resonance structure in the cross-sections of the ionic states of H_2O. More experimental and theoretical study is needed to provide a definitive understanding of the usefulness of the ST model in the prediction and identification of resonances in H_2O.

ACKNOWLEDGEMENTS

This work was supported by the Director, Office of Energy Research, Office of Basic Energy Sciences, Chemical Sciences, Division of the U. S. Department of Energy under Contract No. W-7405-ENG-48. It was performed at the Stanford Synchrotron Radiation Laboratory, which is supported by the NSF Grant No. DMR 77-27489, in cooperation with the Stanford Linear Accelerator Center. We wish to thank Dr. J. J. Delaney for providing us with a pre-print of his ST calculations prior to publication.

REFERENCES

1. C. N. Yang, Phys Rev. 74, 764 (1943).
2. If direct photodissociation accompanies photoionization, there is more information in the correlation of product properties.
3. K. N. Huang, Phys. Rev. A 22, 223 (1980).
4. V. Rehn, A. D. Baer, J. L. Stanford, D. S. Kyser, and V. O. Jones, in "Vacuum Ultraviolet Physics," edited by E. Koch, R. Haensel, and C. Kunz (Braunschweig, Pergammon-Vieweg, 1974), pp. 780-2.
5. M. G. White, R. A. Rosenberg, G. Gabor, E. D. Poliakoff, G. Thornton, S. H. Southworth, and D. A. Shirley, Rev. Sci. Instrum. 50, 1288 (1979).
6. W. H. Hancock and J. A. R. Samson, J. Electron Spectrosc. Relat. Phenom. 9, 211 (1976); J. Kriele and A. Schweig, J. Electron Spectrosc. Relat. Phenom. 20, 191 (1980).
7. F. Wuilleumier and M. O. Krause, J. Electron Spectrosc. Relat. Phenom. 15, 73 (1978). J. L. Dehmer, W. A. Chupka, J. Berkowitz, and W. T. Jivery, Phys. Rev. A. 12, 1966 (1973).
8. S. Southworth, C. M. Truesdale, P. H. Kobrin, D. W. Lindle, W. D. Brewer, and D. A. Shirley, submitted to J. Chem. Phys. (1981).
9. L. de Reilhac and N. Damany, J. Quant. Spectry. Radiative Transfer 18, 121 (1977).
10. D. H. Katayama, R. E. Huffman, and L. L. O'Bryan, J. Chem. Phys. 59, 4309 (1973).
11. T. A. Carlson and G. E. McGuire, J. Electr. Spectr. Relat. Phonom. 1, 209 (1972-73).

12. S. Katsumata, Y. Achiba, and K. Kimura, J. Electron. Spectrosc. Relat. Phenom. 17, 229 (1979).

13. K. H. Tan, C. E. Brion, Ph. E. van der Leeuw, and M. J. van der Wiel, Chem. Phys. 29, 299 (1973).

14. M. Roche, D. R. Salahub, and P. R. Messmer, J. Elect. Spectr. and Relat. Phenom. 19, 273 (1980).

15. M. S. Banna and D. A. Shirley, J. Chem. Phys. 63, 4759 (1975).

16. J. C. Slater, Adv. Quantum Chem. 6, 1 (1972).

17. D. Dill and J. Dehmer, J. Chem. Phys. 61, 692 (1974).

18. G. R. J. Williams and P. W. Langhoff, Chem. Phys. Letters 60, 201 (1979).

19. P. R. Hilton, S. Nordholm, and N. S. Hush, Chem. Phys. Letters 64, 595 (1979).

20. P. W. Langhoff, Chem. Phys. Letters 22, 60 (1973).

21. T. N. Rescigno, C. F. Bender, B. V. McKoy, and P. W. Langhoff, J. Chem. Phys. 63, 970 (1978).

22. J. J. Delaney, V. R. Saunders, and I. H. Hillier, J. Phys. B. Atom. Molec. Phys. 14, 819 (1981).

23. O. Dutuit, K. Ito, A. Tabche-Foutiale, P. Morin, T. Baer, P. M. Guyon, and I. Nenner, Proc. 6th Int. Conf. of Vacuum Ultraviolet radiation Physics, Charlottesville, USA Abstracts 12, 17 (1980).

24. C. Y. R. Wu and D. L. Judge, J. Chem. Phys. 75, 172 (1981).

Table I. Cross sections and asymmetry parameters of the $^2B_1$, $^2A_1$ and $^2B_2$ ionic states of H_2O.

	$^2B_1$		$^2A_1$		$^2B_2$	
hν(eV)	σ(Mb)	β	σ(Mb)	β	σ(Mb)	β
18.	5.60(14)*	.76(5)	6.51(16)	.35(4)	...	...
19.	5.91(15)	.88(5)	5.83(14)	.45(4)	...	...
19.5	5.01(15)	1.18(8)	4.83(14)	.63(6)		
20.	5.24(15)	1.09(6)	4.71(14)	.85(6)	...	...
20.5	5.23(13)	1.08(7)	5.23(13)	.75(5)		
21.2	5.77(14)	.99(8)	5.87(16)	.68(5)	7.03(16)	-.11(3)
	5.9(4)[a]	1.09(4)[a],1.0(1)[b]	6.0(4)[a]	.45(5)[a],.3(1)[b]	8.4(8)[a]	-.09(10)[a],-.1(2)
22	6.06(15)	.96(6)	5.70(15)	.72(5)	8.05(18)	-.10(3)
23	5.92(15)	.96(6)	5.65(14)	.64(5)	7.32(17)	-.06(3)
23.3	5.46(14)	1.06(7)	5.41(14)	.76(6)	7.88(18)	.02(3)
23.5	5.23(13)	1.24(7)	5.00(13)	1.00(5)	6.91(16)	.02(3)
	6.03[c]		5.44[c]		6.63[c]	
24	5.11(14)	1.19(7)	4.77(14)	.85(6)	6.81(17)	.06(3)
24.5	5.23(13)	1.20(7)	4.88(13)	.94(6)	6.69(16)	.20(3)
	5.65[c]		5.30[c]		6.59[c]	
25	6.16(14)	.88(5)	6.00(14)	.75(5)	7.83(17)	.22(3)
26	5.55(15)	1.05(5)	5.03(13)	.90(6)	6.94(17)	.23(4)
27	5.26(13)	1.21(6)	5.45(13)	.80(3)	6.70(15)	.37(4)
28	4.92(14)	1.31(8)	5.14(14)	.85(6)	6.05(15)	.48(5)
29	4.63(13)	1.12(8)	4.66(13)	1.01(7)	5.77(15)	.54(5)
30	4.40(12)	1.38(8)	3.11(13)	1.20(9)	5.43(15)	.55(6)
31	4.38(14)	1.36(9)	3.72(12)	1.21(9)	5.54(15)	.56(5)

*Errors in the last place are given parenthetically.
[a]Reference 12.
[b]Reference 11.
[c]Reference 13.

Table II. Asymmetry parameter differences between the $^2B_1$ and $^2A_2$ ionic states of H_2O.

$h\nu$	$\Delta\beta$(experiment)*	$\Delta\beta$(theory)**
18	.41(4)	.30
20	.24(6)	.30
22	.24(5)	.29
24	.34(6)	.29
26	.15(6)	.25
28	.46(7)	.28
30	.18(8)	.26

*Present results.
**Roche, et al.[14]

FIGURE CAPTIONS

Fig. 1. TOF photoelectron spectrum showing the $^2B_1$, $^2A_1$, and $^2B_2$ ionic states pf H_2O.

Fig. 2. $\sigma(\varepsilon)$ and $\beta(\varepsilon)$ for the $^2B_1$ $(1b_1^{-1})$. For the $\sigma(\varepsilon)$ curves, A is the Xα calculation of Roche, et al., B is the GIPM calculation of Hilton, et al., C is the ST calculation of Williams and Langhoff, D is the ST calculation of Delaney, et al., □ - are the (e,2e) data of Tan, et al., ■ - are the measurements of Dutuit, et al., and ◆ are the present measurements. For the $\beta(\varepsilon)$ curves, the solid curve is the Xα calculation of Roche, et al. and ◆ are the present measurements.

Fig. 3. Photoionization cross-section $\sigma(\varepsilon)$ and photoelectron asymmetry for H_2O^+ $^2A_1$ $(3a_1^{-1})$. The experimental and theoretical results are denoted as in Fig. 2.

Fig. 4. Photoionization cross-section $\sigma(\varepsilon)$ and photoelectron $\beta(\varepsilon)$ for H_2O^+ $^2B_2$ $(1b_2^{-1})$. The experimental and theoretical results are denoted as in Fig. 2.

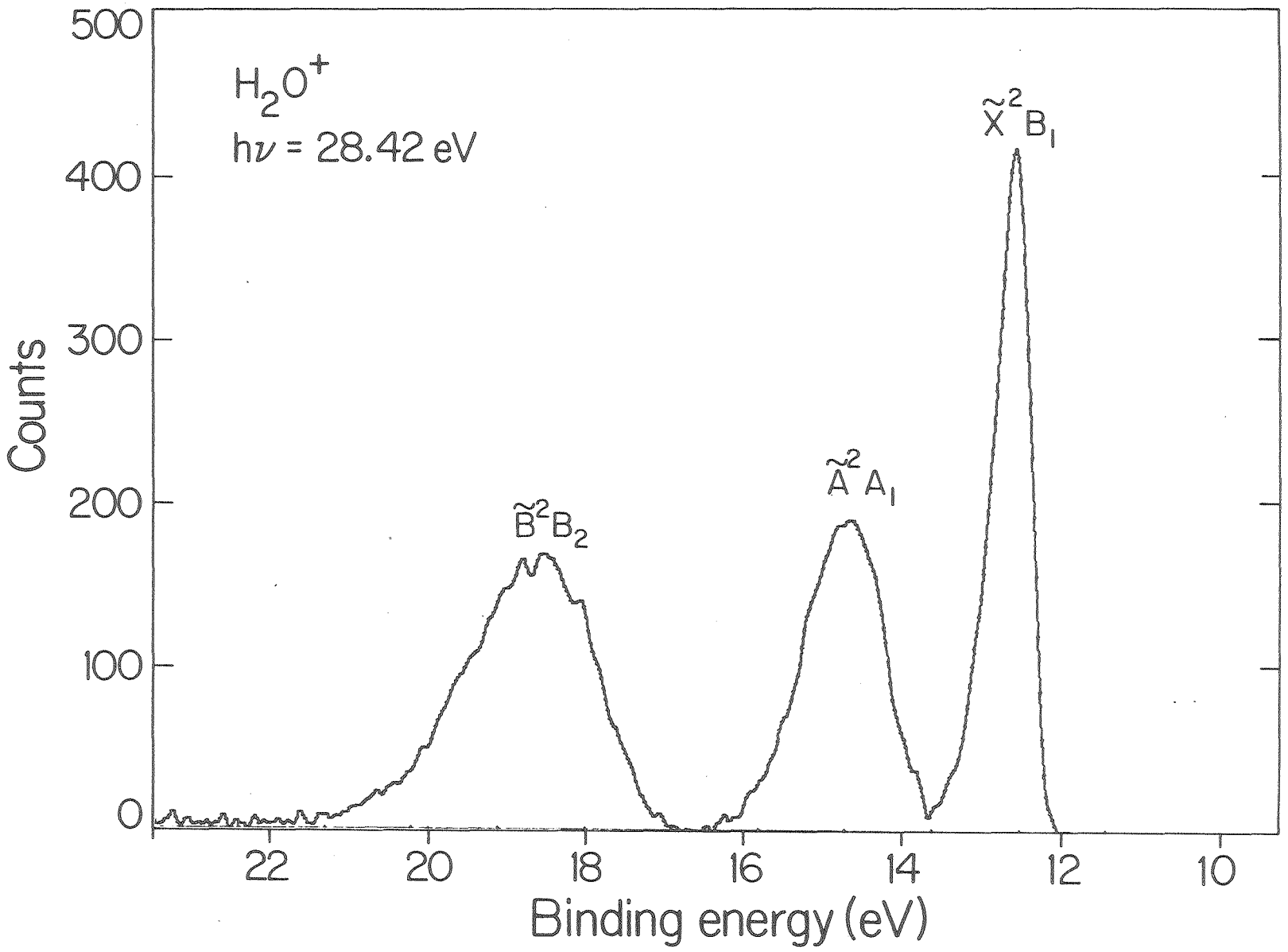

XBL 806-1185

Figure 1

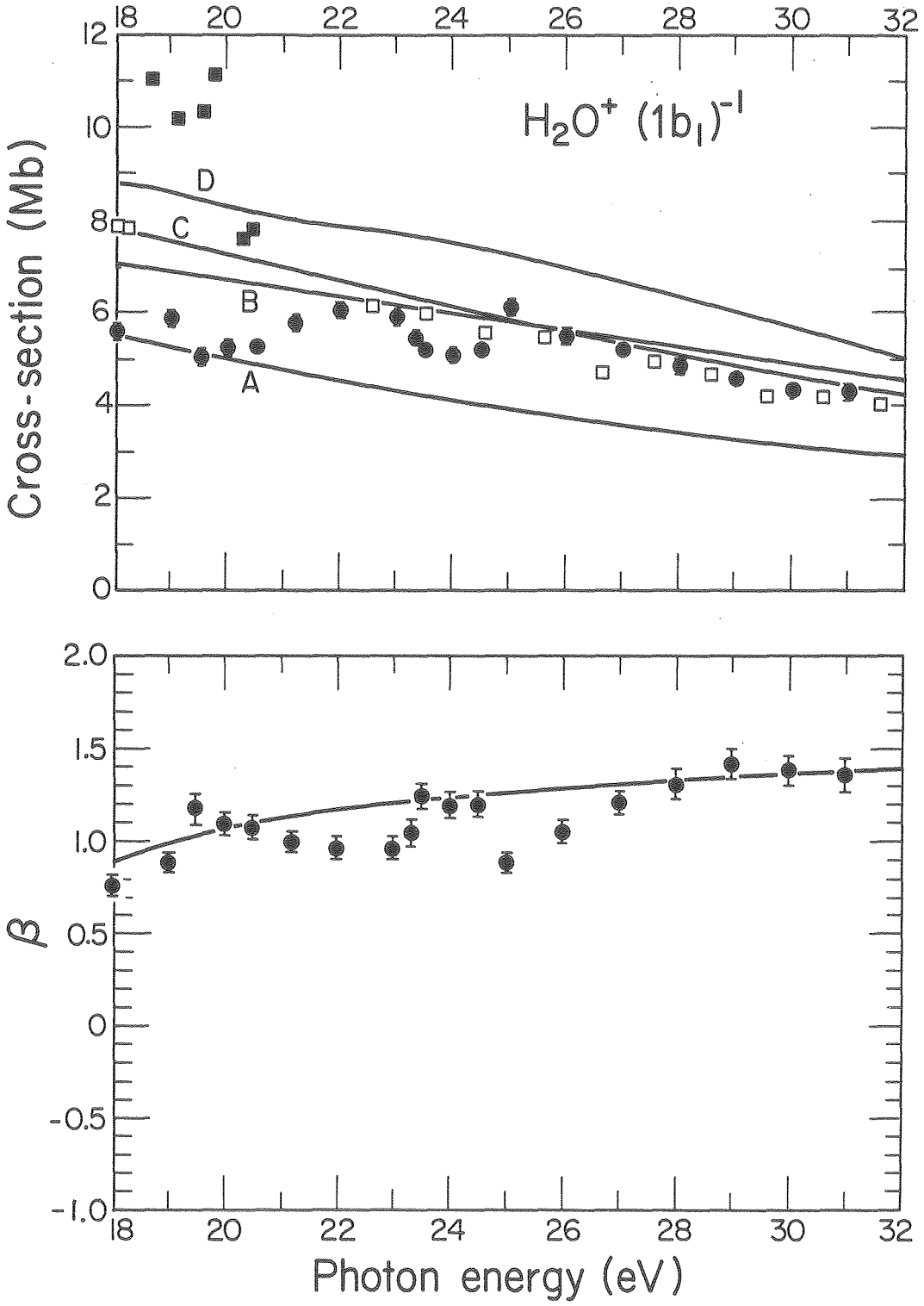
$H_2O^+ (1b_1)^{-1}$
D
C
B
A
Cross-section (Mb)
β
Photon energy (eV)
XBL 818-1224

Figure 2

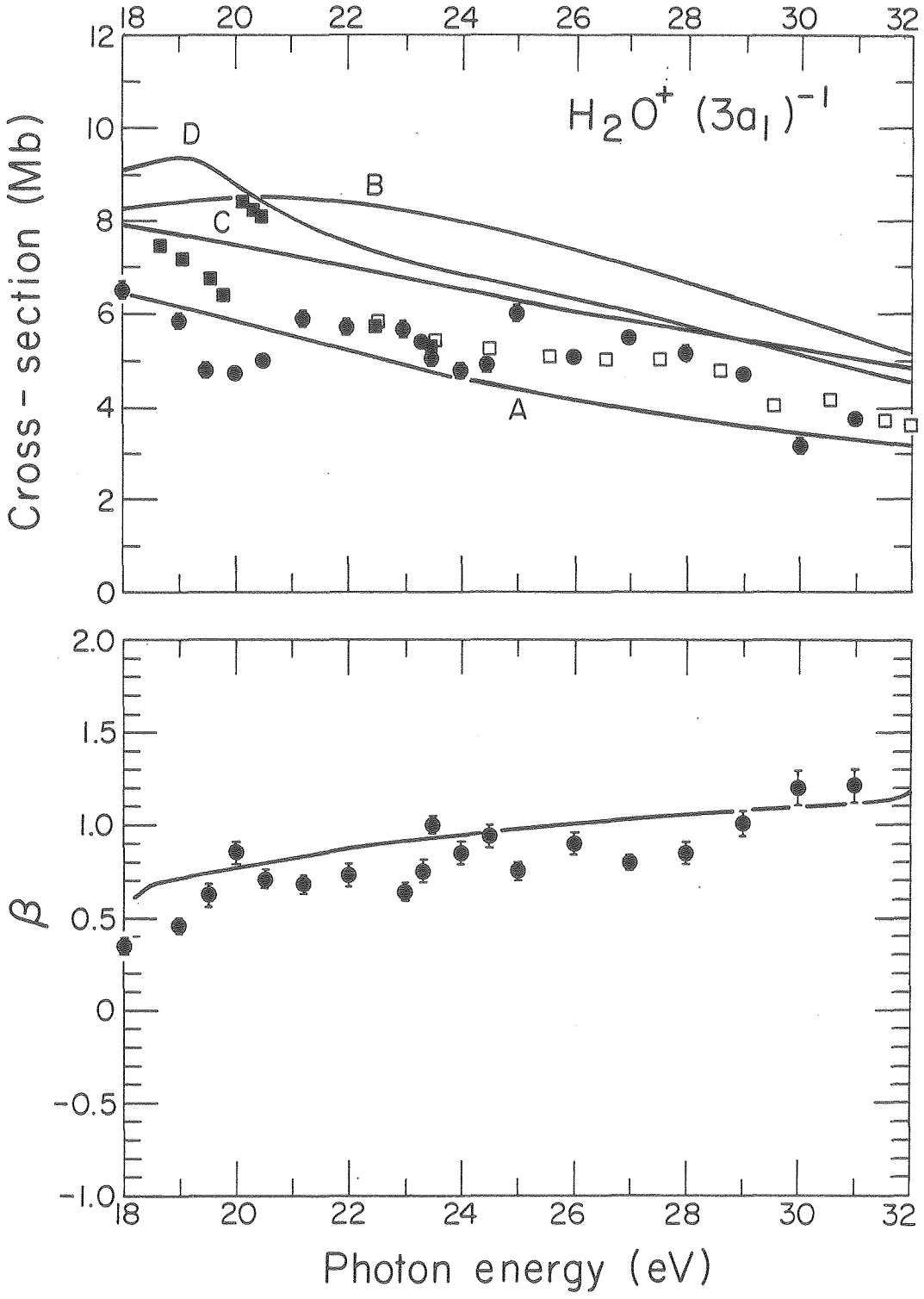

XBL 818-2455

Figure 3

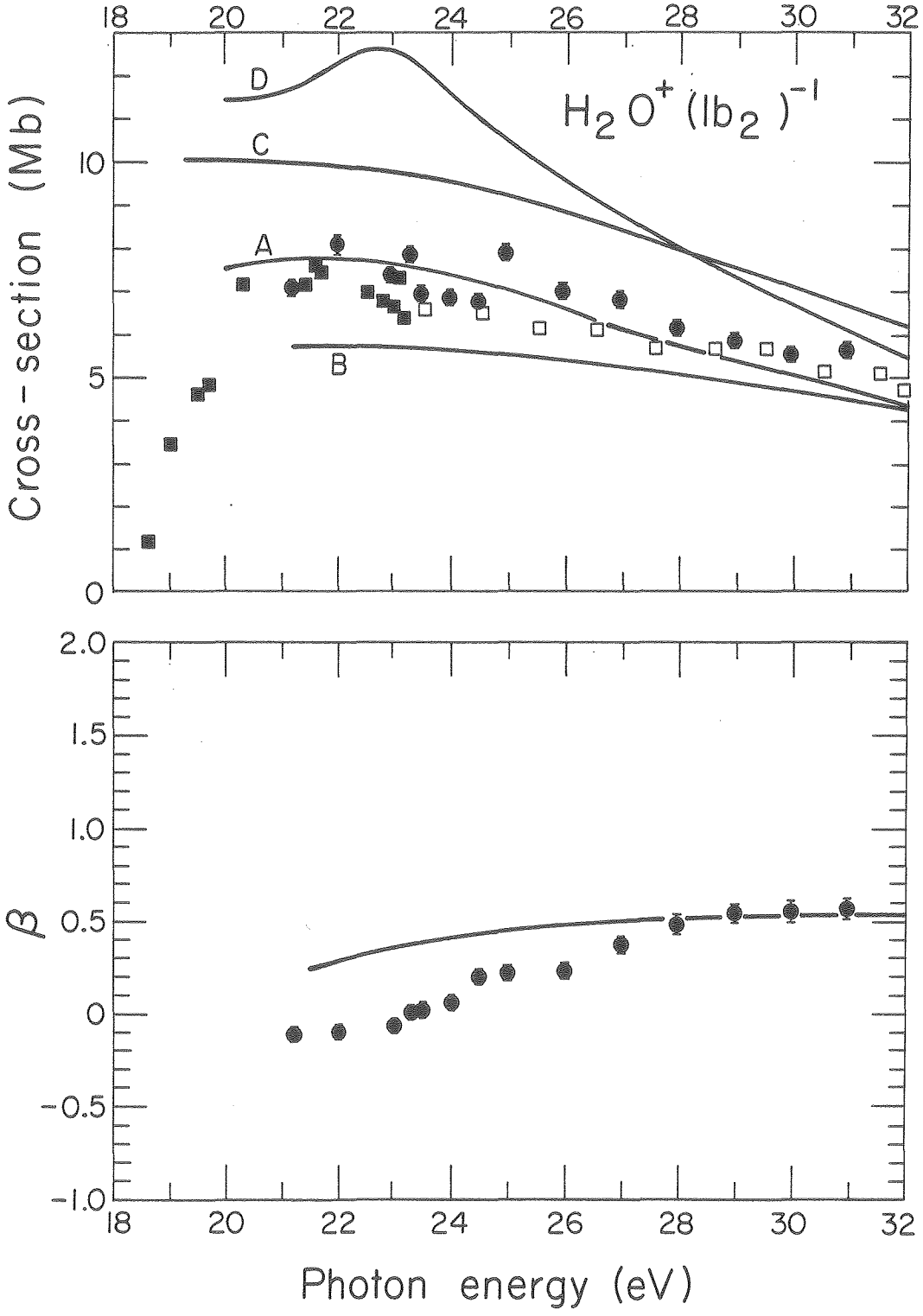

XBL 818-2454

Figure 4